



Quasiparticles in the XXZ model

Ping Lu¹, Gerhard Müller¹, and Michael Karbach^{1,2}

¹ Department of Physics, University of Rhode Island, Kingston RI 02881, USA

² Fachbereich Physik, Bergische Universität Wuppertal, 42097 Wuppertal, Germany

September 15, 2009

The coordinate Bethe ansatz solutions of the XXZ model for a one-dimensional spin-1/2 chain are analyzed with focus on the statistical properties of the constituent quasiparticles. Emphasis is given to the special cases known as XX , XXX , and Ising models, where considerable simplifications occur. The XXZ spectrum can be generated from separate pseudovacua as configurations of sets of quasiparticles with different exclusion statistics. These sets are complementary in the sense that the pseudovacuum of one set contains the maximum number of particles from the other set. The Bethe ansatz string solutions of the XXX model evolve differently in the planar and axial regimes. In the Ising limit they become ferromagnetic domains with integer-valued exclusion statistics. In the XX limit they break apart into hard-core bosons with (effectively) fermionic statistics. Two sets of quasiparticles with spin 1/2 and fractional statistics are distinguished, where one set (spinons) generates the XXZ spectrum from the unique, critical ground state realized in the planar regime, and the other set (solitons) generates the same spectrum from the twofold, antiferromagnetically ordered ground state realized in the axial regime. In the Ising limit, the solitons become antiferromagnetic domain walls.

Key words: XXZ model, Bethe ansatz, string hypothesis, fractional statistics, spinons, solitons.

PACS: 75.10.-b

1. Introduction

Quantum spin chains are physically realized in quasi-one-dimensional magnetic compounds. These are crystalline materials with magnetic ions arranged in exchange-coupled chains that are isolated from each other by non-magnetic ions. The elementary magnetic moments are localized on the sites l of a one-dimensional lattice, which makes them distinguishable. The associated spin operators thus commute if they belong to different sites of that lattice, $[S_l^\alpha, S_{l'}^\beta] = i\hbar\epsilon_{\alpha\beta\gamma}S_l^\gamma\delta_{ll'}$. The Hilbert space of a spin-1/2 chain with N sites is conveniently spanned by product basis vectors $|\sigma_1 \dots \sigma_N\rangle$, $\sigma_l = \uparrow, \downarrow$.

Prominent among the many models employed in the context of quantum spin chain compounds is the spin-1/2 XXZ model,

$$\mathcal{H}_{XXZ} = J \sum_{l=1}^N \{S_l^x S_{l+1}^x + S_l^y S_{l+1}^y + \Delta S_l^z S_{l+1}^z\}. \quad (1)$$

It describes a uniform nearest-neighbor exchange coupling with uniaxial anisotropy. Periodic boundary conditions are assumed. We distinguish ferromagnetic coupling ($J < 0$) from antiferromagnetic coupling ($J > 0$), and the planar regime ($0 \leq \Delta < 1$) from the axial regime ($\Delta > 1$). Important special cases are the XX model ($\Delta = 0$), the XXX model ($\Delta = 1$), and the Ising model ($\Delta \rightarrow \infty$).

One persistent challenge through decades of experiments on quantum spin chain compounds has been the interpretation of the observed intensity spectrum in terms of constituent quasiparticles [1, 2]. The chief motivation of the work reported here is to shed new light on this very issue. The approach taken is eclectic in nature, combining older and more recent results for the unified purpose of understanding the quasiparticle composition of the XXZ spectrum more thoroughly.

The strong interest in the XXZ model is sustained not only by its direct relevance in experimental physics, but also by its amenability to exact analysis via Bethe ansatz. The solution of

the XXZ model was, in fact, the very problem for which Bethe originally invented the method in the early days of quantum mechanics [3, 4]. The Bethe ansatz allows for a characterization of all many-body eigenstates as composed of quasiparticles that scatter off each other or form bound states and thus turn into different quasiparticles. Over the years the same basic idea has been successfully applied to many different kinds of systems and situations including interacting boson and fermion gases with contact interactions [5, 6, 7], the Hubbard model for electrons on a lattice with on-site repulsion [8, 9], and for bosonic and fermionic quantum field theories including the quantum Sine-Gordon and Thirring models [10].

The XXZ spectrum can be generated from different pseudovacua by the systematic creation of quasiparticles with different exclusion statistics. In most cases these pseudovacua are states of lowest energy (physical vacua). An overview of the different kinds of quasiparticles that have emerged from analytic work on the XXZ model is shown in Fig. 1. The boxes in the top row represent quasiparticles whose names are derived from jargon used to describe coordinate Bethe ansatz solutions. These quasiparticles are characterized by strings of complex momenta with common real part and different imaginary parts [7]. One-strings are unbound magnons, two-strings are bound magnon pairs etc. Small (large) imaginary parts indicate loose (tight) binding [11]. At $\Delta = 1$ the strings are constituent particles of (degenerate) multiplets of eigenstates with total spin S_T . These multiplets split up energetically at $\Delta \neq 1$.

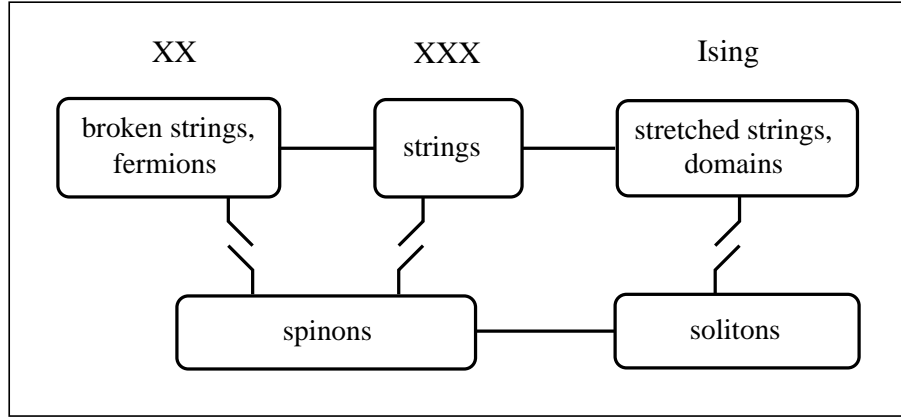


Figure 1. Zoo of quasiparticles that play some role in the context of the XXZ model. For $J > 0$, the pseudovacua of spinons and solitons are at the bottom of the spectrum. The pseudovacuum of the string particles is at the top in the axial regime ($\Delta \geq 1$) and moves downward in the planar regime ($0 \leq \Delta \leq 1$), reaching the center in the XX limit and coinciding there with the pseudovacuum of Jordan-Wigner fermions.

At $\Delta = 0$ the energy levels join up in new degenerate configurations, reflecting different symmetries [12, 13, 14, 15, 16, 17]. A more natural classification scheme for the XX spectrum is then based on string fragments. Hence the name *broken strings*. These fragments are closely related to the free lattice fermions that emerge from the Jordan-Wigner representation of spin-1/2 operators [12, 15, 16, 17]. At $\Delta > 1$ the imaginary parts of the string solutions grow in magnitude and diverge as $\Delta \rightarrow \infty$. Hence the name *stretched strings*. The tightly bound strings are related, in the Ising limit, to localized domains of reversed spins on successive lattice sites. The exclusion statistics of these domains is similar to yet subtly different from that of the strings.

The boxes in the bottom row of Fig. 1 represent quasiparticles that are complementary to the string particles. The string pseudovacuum contains the maximum number of spinons or solitons. The spinon and soliton vacua contain strings at maximum capacity. Whereas the string particles have integer-valued exclusion statistics, the spinons and solitons are realizations of fractional statistics [18]. They are both semions but with different pseudovacua. The exclusion principle for semions is, roughly speaking, halfway between those applicable for fermions and bosons. If it takes $1/g$ particles to lower the number of orbitals in a band available for occupancy by one, then $g = 1$

describes fermions, $g = 1/2$ semions, and $g = 0$ bosons (as a limit).

The string particles and the semionic particles are natural building blocks for the systematic construction of a complete XXZ eigenbasis from different pseudovacua. The configurations of string particles and semionic particles are both unique and preserved in every XXZ eigenstate. The ground state (physical vacuum) of the XXZ antiferromagnet ($J > 0$) coincides with the pseudovacua of the semions. The spinon vacuum is unique and coincides with the non-degenerate ground state of the XXZ model at $0 \leq \Delta \leq 1$ for even N . The soliton vacuum is twofold and coincides with the ground state of the XXZ model at $\Delta > 1$ for $N \rightarrow \infty$.

Let us briefly illustrate the relation between the particles from the top and bottom rows in Fig. 1 with two simple scenarios, one in configuration space and the other in momentum space. In the Ising limit, \mathcal{H}_{XXZ} has simple product eigenstates. The ferromagnetic state $|\uparrow\uparrow\uparrow\cdots\rangle$ is the unique pseudovacuum for domains of consecutive flipped spins, $\downarrow\downarrow\cdots\downarrow$, as shown in top part of Fig. 2. The twofold Néel state, $|\uparrow\downarrow\uparrow\cdots\rangle$, $|\downarrow\uparrow\downarrow\cdots\rangle$, by contrast, is the pseudovacuum for antiferromagnetic domain walls of the kind $\uparrow\uparrow$, $\downarrow\downarrow$ as shown in the bottom part of Fig. 2. These domain walls (named solitons) have effective spin $\pm 1/2$. The integer-valued exclusion statistics of domains is associated with the fact that neighboring particles must be separated by any positive integer number of lattice sites. The fractional exclusion statistics of domain walls, on the other hand, is associated with the fact that one of two lattice sites may be shared by neighboring particles.

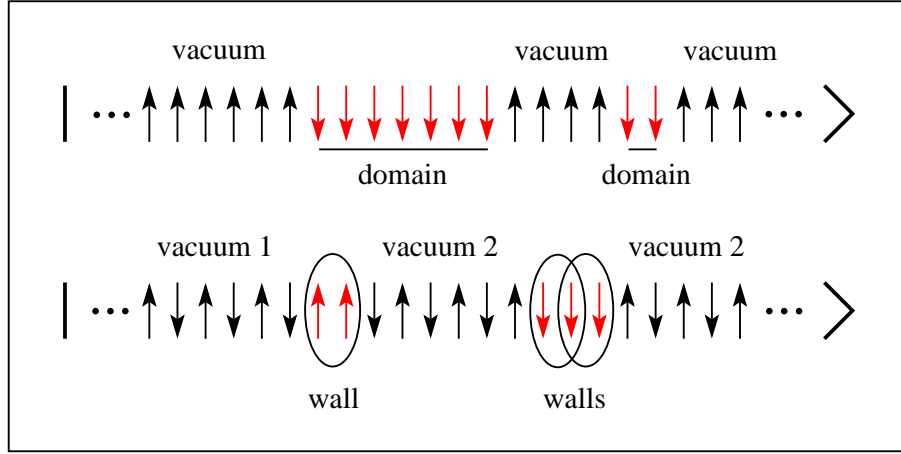


Figure 2. Constituent quasiparticles of \mathcal{H}_{XXZ} at $\Delta \rightarrow \infty$ in real space (lattice of N sites). They are either domains of flipped spins embedded in the unique vacuum with all spins up (top) or domain walls embedded in the twofold vacuum with all spins alternatingly up/down (bottom).

In the XX limit, \mathcal{H}_{XXZ} is equivalent to a system of N_F free lattice fermions in a band [19, 20, 21, 22]. The ground state corresponds to the intact Fermi sea at $|k| < k_F$ as shown in Fig. 3. The entire spectrum can be generated systematically via particle excitations ($\Delta N_F = +1$), hole excitations ($\Delta N_F = -1$), and particle-hole excitations ($\Delta N_F = 0$). The Fermi-sea ground state can be viewed as the pseudovacuum for semionic spinons. We introduce a threshold momentum k_c that varies with N_F . When a fermion is removed from the intact sea, k_c slightly increases to generate not just one but two vacancies in the interval $|k| < k_c$ of the band. These two holes are then identified with a pair of spin-up spinons. When a fermion is added outside the intact Fermi sea, k_c slightly decreases to produce two particles in the region $|k| > k_c$. They are identified with a pair of spin-down spinons. A fermionic particle-hole excitation leaves k_c unchanged and is interpreted as a pair of spinons with opposite spin orientation. The entire spectrum can thus be described in the form of spinon configurations.

The main goal of this work is to identify the relationship between the string particles and the semionic particles for \mathcal{H}_{XXZ} at $\Delta = 0, 1, \infty$ in particular and to illuminate how this relationship can be tracked between the three points in parameter space. In Sec. 2 we set the stage for this investigation by reviewing the relevant Bethe-ansatz representations that best serve our purpose.

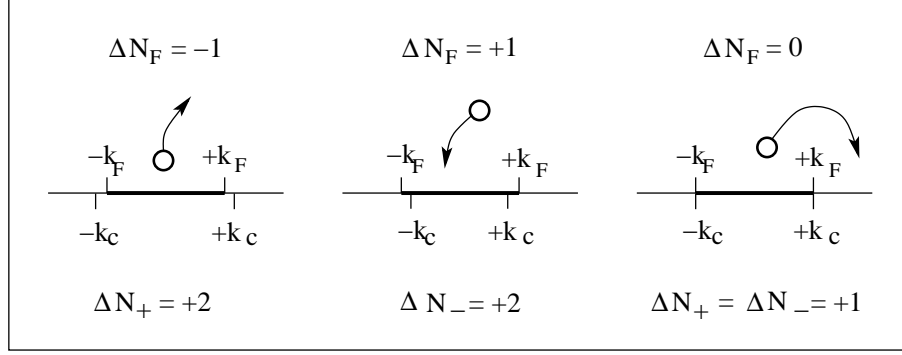


Figure 3. Constituent quasiparticles of \mathcal{H}_{XXZ} at $\Delta = 0$ in reciprocal space (fermionic band with Fermi momentum k_F). They are either spinless Jordan-Wigner fermion or semionic spinons with spin $\pm 1/2$.

We then discuss the quasiparticle composition of the XXZ spectrum in the XXX limit (Sec. 3.1), the Ising limit (Sec. 3.2), and the XX limit (Sec. 3.3).

2. Bethe ansatz

The coordinate Bethe ansatz for \mathcal{H}_{XXZ} uses the magnon vacuum $|F\rangle \equiv |\uparrow\uparrow\cdots\uparrow\rangle$ with energy $E_F = JN\Delta/4$ as its reference state. The Bethe form [3] of any eigenvector in the invariant subspace with magnetization $M_z = N/2 - r$,

$$|\psi\rangle = \sum_{1 \leq n_1 < \dots < n_r \leq N} a(n_1, \dots, n_r) S_{n_1}^- \cdots S_{n_r}^- |F\rangle, \quad (2)$$

has coefficients of the form

$$a(n_1, \dots, n_r) = \sum_{\mathcal{P} \in S_r} \exp \left(i \sum_{j=1}^r k_{\mathcal{P}j} n_j + \frac{i}{2} \sum_{i < j}^r \theta_{\mathcal{P}i \mathcal{P}j} \right), \quad (3)$$

determined by r magnon momenta k_i and one phase angle, $\theta_{ij} = -\theta_{ji}$, for each magnon pair. The sum $\mathcal{P} \in S_r$ is over the permutations of the indices $\{1, 2, \dots, r\}$. The k_i and θ_{ij} satisfy the Bethe ansatz equations (BAE),

$$e^{iNk_i} = \prod_{j \neq i}^r e^{i\theta_{ij}}, \quad e^{i\theta_{ij}} = -\frac{e^{i(k_i+k_j)} + 1 - 2\Delta e^{ik_i}}{e^{i(k_i+k_j)} + 1 - 2\Delta e^{ik_j}}. \quad (4)$$

The energy and the wave number of an eigenstate with magnon momenta $\{k_1, \dots, k_r\}$ are

$$\frac{E - E_F}{J} = \sum_{i=1}^r (\cos k_i - \Delta), \quad k = \left(\sum_{i=1}^r k_i \right) \bmod(2\pi). \quad (5)$$

Reasons of practicality dictate the use of different transformations of the BAE in the regimes of axial anisotropy ($\Delta > 1$), planar anisotropy ($\Delta < 1$), and isotropic exchange ($\Delta = 1$). It is convenient to introduce rapidities z_i ,

$$\cot \frac{k_i}{2} = \begin{cases} \cot \frac{\gamma}{2} \tanh \frac{\gamma z_i}{2} & : 0 \leq \Delta = \cos \gamma < 1 \\ z_i & : \Delta = 1 \\ \coth \frac{\eta}{2} \tan \frac{\eta z_i}{2} & : \Delta = \cosh \eta > 1 \end{cases}, \quad (6)$$

which renders the limit $\Delta \rightarrow 1$ smooth from both sides. The BAE (4) thus transform into

$$N\tilde{\phi}_1(z_i) = 2\pi I_i + \sum_{j \neq i}^r \tilde{\phi}_2(z_i - z_j), \quad i = 1, \dots, r, \quad (7)$$

where

$$\tilde{\phi}_\nu(z) \doteq \begin{cases} 2 \arctan \left(\cot \frac{\gamma\nu}{2} \tanh \frac{\gamma z}{2} \right) & : 0 \leq \Delta < 1 \\ 2 \arctan \frac{z}{\nu} & : \Delta = 1 \\ 2 \arctan \left(\coth \frac{\eta\nu}{2} \tan \frac{\eta z}{2} \right) & : \Delta > 1 \end{cases}. \quad (8)$$

The Bethe quantum numbers (BQN) I_i of integer or half-integer value reflect the multivaluedness of the logarithm used in the transformation. They are subject to restrictions that will be discussed case by case. The energy expression in (5) becomes

$$\frac{E - E_F}{J} = - \sum_{i=1}^r \tilde{e}(z_i), \quad \tilde{e}(z) \doteq \begin{cases} \frac{\sin^2 \gamma}{\cosh(\gamma z) - \cos \gamma} & : 0 \leq \Delta < 1 \\ \frac{2}{1 + z^2} & : \Delta = 1 \\ \frac{-\sinh^2 \eta}{\cos(\eta z) - \cosh \eta} & : \Delta > 1 \end{cases}. \quad (9)$$

Note that we are, effectively, dealing with a single anisotropy parameter, $\eta = \nu\gamma$, that is real in one regime, imaginary in the other, and zero at the isotropy point. This parametrization is particularly useful for tracking the spectrum between the axial and planar regimes across the point of higher rotational symmetry. Slightly different parametrizations are more adequate for the exploration of the limits $\Delta \rightarrow \infty$ in the axial regime and $\Delta \rightarrow 0$ in the planar regime.

2.1. Axial regime

At $\Delta > 1$ we use the transformation [23],

$$\tan \frac{z_i}{2} \doteq \tanh \frac{\eta}{2} \cot \frac{k_i}{2}, \quad \eta = \text{arcosh } \Delta, \quad -\pi < z_i < \pi, \quad (10)$$

instead of (6), to bring the BAE (4) into the form

$$\left(\frac{\coth(\eta/2) \tan(z_i/2) - \imath}{\coth(\eta/2) \tan(z_i/2) + \imath} \right)^N = \prod_{j \neq i}^r \frac{\coth(\eta) \tan[(z_i - z_j)/2] - \imath}{\coth(\eta) \tan[(z_i - z_j)/2] + \imath}, \quad i = 1, \dots, r. \quad (11)$$

The associated trigonometric BAE are

$$N\phi_1(z_i) = 2\pi I_i + \sum_{j \neq i}^r \phi_2(z_i - z_j), \quad i = 1, \dots, r, \quad (12)$$

where

$$\phi_\nu(z) \doteq 2 \arctan \left(\frac{\tan(z/2)}{\tanh(\eta\nu/2)} \right) + 2\pi \left\lfloor \frac{\Re z}{2\pi} + \frac{1}{2} \right\rfloor. \quad (13)$$

The second term in (13) ensures that the set $\{I_i\}$ remains the same as an eigenstate is tracked across the axial regime [7]. Here $\lfloor x \rfloor$ is the floor function (integer part of x).

For the analysis of solutions that include complex magnon momenta we invoke the string hypothesis for the rapidities [7]:

$$z_\alpha^{m,l} = z_\alpha^m + \imath\eta(m+1-2l), \quad l = 1, \dots, m, \quad m = 1, 2, \dots, r. \quad (14)$$

The index l distinguishes rapidities belonging to the same string (of size m). The index $\alpha = 1, \dots, n_m$ distinguishes different strings of the same size. The string ansatz (14) produces only asymptotic solutions of the BAE (11) for $N \rightarrow \infty$. The finite- N corrections are, in general, exponentially small, and not all finite- N solutions fit the string template (14) [7]. However, neither corrections nor exceptions affect macroscopic systems. In the Ising limit, where the spread of imaginary parts in (14) diverges, all corrections and exceptions disappear even for finite N .

A given string solution of (11) with magnetization $M_z = N/2 - r$ is described by r rapidities that breaks down into configurations of strings such that the constraint,

$$\sum_{m \in \mathcal{C}} m n_m = r, \quad (15)$$

is satisfied, where the set \mathcal{C} identifies those sizes of strings that occur in a given eigenstate. With the functions

$$\varphi_\nu(z) \doteq \frac{\coth(\eta\nu/2) \tan(z/2) - i}{\coth(\eta\nu/2) \tan(z/2) + i} = \frac{\sin((z - i\eta\nu)/2)}{\sin((z + i\eta\nu)/2)} \quad (16)$$

we rewrite Eqs. (11) in the form

$$[\varphi_1(z_i)]^N = \prod_{j \neq i}^r \varphi_2(z_i - z_j), \quad i = 1, \dots, r. \quad (17)$$

When we substitute the string ansatz (14) into Eqs. (17) we obtain

$$[\varphi_1(z_\alpha^{m,l})]^N = \prod_{(m',\beta) \neq (m,\alpha)} \prod_{k=1}^{m'} \varphi_2(z_\alpha^{m,l} - z_\beta^{m',k}) \prod_{k \neq l}^m \varphi_2(z_\alpha^{m,l} - z_\alpha^{m,k}), \quad (18)$$

for $l = 1, \dots, m$ and $\alpha = 1, \dots, n_m$, where

$$\varphi_\nu(z_\alpha^{m,l}) = \frac{\sin([z_\alpha^m + i\eta(m+1-\nu-2l)]/2)}{\sin([z_\alpha^m + i\eta(m+1+\nu-2l)]/2)}. \quad (19)$$

To determine the real parts, z_α^m , we form the product of all Eqs. (18) for fixed m, α :

$$\left[\prod_{l=1}^m \varphi_1(z_\alpha^{m,l}) \right]^N = \prod_{(m',\alpha') \neq (m,\alpha)} \left[\prod_{k=1}^{m'} \prod_{l=1}^m \varphi_2(z_\alpha^{m,l} - z_{\alpha'}^{m',k}) \right] \left[\prod_{l=1}^m \prod_{k \neq l}^m \varphi_2(z_\alpha^{m,l} - z_\alpha^{m,k}) \right]. \quad (20)$$

Each expression in square brackets can be simplified massively, producing the BAE for the z_α^m ,

$$[\varphi_n(z_\alpha^m)]^N = \prod_{(m',\alpha') \neq (m,\alpha)} \varphi_{m'-m}(z_{\alpha\alpha'}^{mm'}) \varphi_{m'+m}(z_{\alpha\alpha'}^{mm'}) \prod_{l=1}^{m-1} \left[\varphi_{m'+m-2l}(z_{\alpha\alpha}^{mm'}) \right]^2, \quad (21)$$

with $z_{\alpha\alpha'}^{mm'} \doteq z_\alpha^m - z_{\alpha'}^{m'}$. The associated trigonometric BAE,

$$N\phi_m(z_\alpha^m) = 2\pi I_\alpha^m + \sum_{(m',\alpha') \neq (m,\alpha)} \Phi_{mm'}(z_{\alpha\alpha'}^{mm'}), \quad (22)$$

$$\Phi_{mm'}(z) \doteq \begin{cases} \phi_{|m-m'|}(z) + 2\phi_{|m-m'|+2}(z) + \dots + 2\phi_{m+m'-2}(z) + \phi_{m+m'}(z) & : m' \neq m \\ 2\phi_2(z) + 2\phi_4(z) + \dots + 2\phi_{2m-2}(z) + \phi_{2m}(z) & : m' = m \end{cases}, \quad (23)$$

depend on a set $\{I_\alpha^m\}$ of BQN that reflects the specific string combination of any given eigenstate. The energy and wave number of that state are

$$\frac{E - E_F}{J} = - \sum_{(m,\alpha)} \frac{\sinh \eta \sinh(\eta m)}{\cosh(\eta m) - \cos z_\alpha^m}, \quad k = \left[\sum_{(m,\alpha)} \left(\pi - \frac{2\pi}{N} I_\alpha^m \right) \right] \bmod(2\pi). \quad (24)$$

The range of the I_α^m will be discussed first for the case $\Delta = 1$ in Sec. 2.2 and then for the axial regime including the Ising limit in Sec. 3.2.

2.2. Isotropic exchange

At $\Delta = 1$ we retain the rapidities from (6), the trigonometric BAE in the form (7), and the energy expression (9). The string hypothesis now reads

$$z_\alpha^{m,l} = z_\alpha^m + i(m+1-2l), \quad l = 1, \dots, m, \quad m = 1, 2, \dots, r. \quad (25)$$

The BAE for the real parts z_α^m are Eqs. (21) with (19) replaced by

$$\varphi_\nu(z_\alpha^{m,l}) = \frac{z_\alpha^m + i(m+1-\nu-2l)}{z_\alpha^m + i(m+1+\nu-2l)}. \quad (26)$$

The associated trigonometric BAE for the z_α^m then take on the form (22) with $\Phi_{mm'}(z)$ from (23) and $\phi_\nu(z) \doteq 2 \arctan(z/\nu)$ from (8). The energy and wave number of an eigenstate specified by the set $\{I_\alpha^m\}$ are

$$\frac{E - E_F}{J} = - \sum_{(m,\alpha)} \frac{2m}{m^2 + (z_\alpha^m)^2}, \quad k = \left[\sum_{(m,\alpha)} \left(\pi - \frac{2\pi}{N} I_\alpha^m \right) \right] \bmod(2\pi). \quad (27)$$

The string hypothesis sets the range of the I_α^m (with $I_{\alpha+1}^m > I_\alpha^m$ implied) as follows [7]:

$$|I_\alpha^m| \leq \frac{1}{2} \left(N - 1 - \sum_{m' \in \mathcal{C}} t_{mm'} n_{m'} \right), \quad t_{mm'} \doteq 2 \min(m, m') - \delta_{mm'}, \quad (28)$$

where n_m is the number of m -strings (distinguished by running index α) in the eigenstate. Note that the range of allowed values becomes narrower for all sizes if a string of any size is added. The I_α^m for a given combination $\{n_m\}$ and a given value of m are either all integers or all half-integers such that the border values of the range (28) are realized.

The Bethe state characterized by a set $\{I_\alpha^m\}$ is the highest-weight component (i.e. the state with $M_z = S_T$) of an S_T -multiplet with total spin

$$S_T = \frac{N}{2} - r, \quad r = \sum_{m \in \mathcal{C}} m n_m. \quad (29)$$

The other components of any given S_T -multiplet are generated by the addition of magnons with zero momentum. These have no effect on the energy or the wave number. Consider the case of a highest-weight state with total spin (29) that only contains 1-strings. Suppose this state is specified by the following set of BQN subject to the constraint (28):

$$-\frac{1}{2}(N-r-1) \leq I_1^1 < \dots < I_r^1 \leq \frac{1}{2}(N-r-1). \quad (30)$$

The rapidities z_α^1 derived from the BAE (22),

$$N \phi_1(z_\alpha^1) = 2\pi I_\alpha^1 + \sum_{\beta \neq \alpha}^r \phi_2(z_\alpha^1 - z_\beta^1), \quad \alpha = 1, \dots, r, \quad (31)$$

are real and, with rare exceptions, finite. The member state with $M_z = S_T - 1$ of the same multiplet has one extra rapidity, $z_{r+1} = \infty$, representing the additional magnon with $k_{r+1} = 0$. The BAE (22) for this state are then satisfied with the same z_α^1 , $\alpha = 1, \dots, r$ and with $z_{r+1} = \pm\infty$ if we set the BQN as follows:

$$\tilde{I}_\alpha^1 = I_\alpha^1 \pm \frac{1}{2}, \quad \alpha = 1, \dots, r; \quad \tilde{I}_{r+1}^1 = \pm \frac{1}{2}(N - r). \quad (32)$$

In the more general case, where the highest-weight state under consideration contains strings with $m > 1$, the shifts in the already existing BQN, I_α^m , and the value of the new BQN, I_{r+1}^1 , will be different. In Sec. 3.1 we will treat the strings as interacting particles and examine their exclusion statistics.

2.3. Planar regime

The string ansatz at $\Delta < 1$ [7] will not be used here. Simplifications and residual complications that occur in the limit $\Delta \rightarrow 0$ can be seen in the raw form (4) of the BAE. There are two categories of solutions, both of which are ubiquitous. Regular and singular solutions are distinguished by the absence or presence of pairs of critical magnon momenta with $k_i + k_j = \pi$, which make both the numerator and the denominator in (4) vanish as $\Delta \rightarrow 0$.

All regular solutions produce real magnon momenta from $e^{iNk_i} = (-1)^{r-1}$, whereas singular solutions include critical magnon pairs that are either both real or form a complex-conjugate pair [12, 15, 16, 17]. The latter can be interpreted as fragments of strings that exist throughout the planar regime. Since all critical pairs are associated with a twofold degeneracy of eigenstates with equal wave number, the singular features as imposed by the BAE in the limit $\Delta \rightarrow 0$ can be removed by unitary transformations. This erases, at $\Delta = 0$, all traces of the string nature, at $\Delta > 0$, of complex solutions. The magnon momenta thus regularized are

$$k_\alpha = \pi - \frac{2\pi}{N} I_\alpha^1. \quad (33)$$

The associated BQN are integers for odd r and half-integers for even r with range

$$|I_\alpha^1 - \tau_r| \leq \frac{1}{2}(N - 1), \quad \tau_r = \frac{1}{2}[1 - (-1)^r]. \quad (34)$$

Their relation to the BQN (28) and (32) of the S_T -multiplet states will be discussed in Sec. 3.3.

The regularized BAE solutions (33) describe hard-core bosons. The phase shift is $\theta_{ij} = \pi$ for all two-particle interactions. These hard-core bosons are equivalent to the Jordan-Wigner fermions [19, 20, 21, 22] that have been instrumental in most studies of the XX model.

3. Quasiparticle composition of XXZ spectrum

We are now ready to explore the relationship between the complementary quasiparticle compositions of the XXZ spectrum. We begin in Sec. 3.1 with string particles and the complementary spinon particles for the XXX case. In Sec. 3.2 we then discuss the effects of axial anisotropy on the strings and their relationship to ferromagnetic domains in the Ising limit. Complementary to these domains are the soliton particles in the shape of antiferromagnetic domain walls. In the planar regime the strings evolve differently. What remains of them in the XX limit are fragments that act like hard-core bosons or, equivalently, free Jordan-Wigner fermions. Complementary to the latter are again the spinons as will be discussed in Sec. 3.3.

3.1. XXX limit: strings and spinons

The very structure of the coordinate Bethe ansatz suggests that the strings (25) can be interpreted as quasiparticles. There exists a universal energy-momentum relation as implied by (27).

The particle interaction is encoded in the set of momenta (or rapidities) dictated by the BAE and in the phase shifts associated with elastic two-particle collisions.

The exclusion statistics of strings is determined by the rule (28) governing the range of BQN and by the relation (29) governing the capacity for strings in a highest-weight state of given S_T . The total number of S_T -multiplets with string content $\{n_1, n_2, \dots\}$ becomes the solution of a standard combinatorial problem:

$$W(\{n_m\}) = \prod_{m \in \mathcal{C}} \binom{d_m + n_m - 1}{n_m}, \quad d_m = A_m - \sum_{m' \in \mathcal{C}} g_{mm'}(n_{m'} - \delta_{mm'}), \quad (35)$$

where

$$A_m = N + 1 - 2m, \quad g_{mm'} = 2 \min(m, m') \quad (36)$$

are statistical capacity constants and statistical interaction coefficients, respectively, that are specific to the string particles [13, 18, 24, 25, 26]. Taking into account the $(2S_T + 1)$ -fold degeneracy of each multiplet, this classification accounts for the complete spectrum,

$$\sum_{\{n_m\}} W(\{n_m\})(2S_T + 1) = 2^N, \quad (37)$$

with the dependence of S_T on $\{n_m\}$ given in (29).

To illustrate the string composition of the XXX spectrum and to explain its relationship to the complementary spinon composition we consider a chain of $N = 6$ sites. In Table 1 we list all combinations $\{n_m\}$ permitted by (29). Also listed is the range of all I_α^m present in each combination as inferred from (28). The distinct configurations of I_α^m thus allowed produce the highest-weight states of all S_T -multiplets as shown in Fig. 4 (left). The quantum number S_T depends on the combinations $\{n_m\}$ via (29) and the wave number k depends on the configurations $\{I_\alpha^m\}$ via (27). Each row of I_α^m in Fig. 4 (left) represents the distinct string motif of an S_T -multiplet. The solution of the BAE (22) thus specified is for the highest-weight component of the multiplet. The non-highest-weight components are characterized by additional BQN as described at the end of Sec. 2.2. The role of these additional BQN will be discussed in Sec. 3.2 for $\Delta > 1$ (see Fig. 5) and in Sec. 3.3 for $\Delta < 1$ (see Fig. 6).

Table 1. String composition $\{n_m\}$ of all S_T -multiplets for $N = 6$. Each row describes a distinct combination for a total of 7. Each combination produces W multiplets for a total of 20. Each multiplet represents $2S_T + 1$ states for a total of 64. Associated with each string in a given combination is a BQN I_α^m of the range shown.

r	\mathcal{C}	n_m	W	$2S_T + 1$	BQN
0	—	—	1	7	—
1	{1}	1	5	5	$ I_\alpha^1 \leq 2$
2	{1}	2	6	3	$ I_\alpha^1 \leq \frac{3}{2}$
2	{2}	1	3	3	$ I_\alpha^2 \leq 1$
3	{1}	3	1	1	$ I_\alpha^1 \leq 1$
3	{1, 2}	1, 1	3	1	$ I_\alpha^1 \leq 1, I_\alpha^2 = 0$
3	{3}	1	1	1	$ I_\alpha^3 = 0$

Elements of the string motif serve as the template of the spinon motif of the same S_T -multiplet. Spinons are specified by their spin and momentum quantum numbers. The spinon interaction depends on the particle momenta and (in general) also on the particle spins. The unique XXX ground state for even N is the spinon vacuum. The ground state for odd N is fourfold degenerate and contains exactly one spinon. The total number N_s of spinon is restricted to be even (odd) for even (odd) N and can assume the values $0 \leq N_s \leq N$. Counting the spin-up spinons (N_+) and spin-down spinons (N_-) separately produces the relations

$$N_+ + N_- = N_s, \quad N_+ - N_- = 2M_z. \quad (38)$$

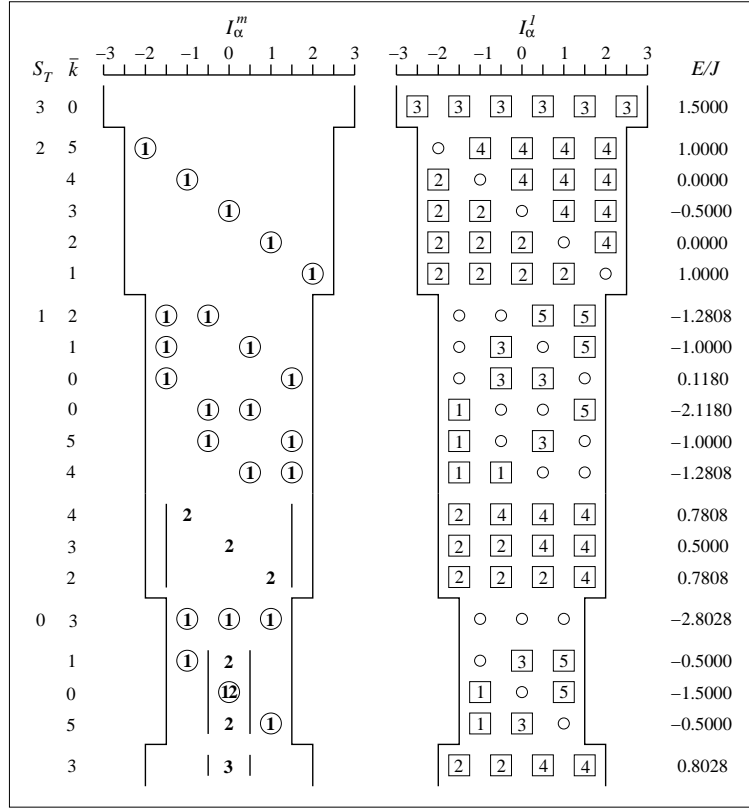


Figure 4. Specification of all S_T -multiplets of the XXX model for $N = 6$ in the string representation (left) and spinon representation (right). The quantum numbers S_T and $\bar{k} \doteq Nk/2\pi$ of each multiplet are stated on the far left. The positions of the numbers $m = 1, 2, 3$ and the vertical lines (left) mark the values of the I_α^m and their range. The I_α^l , emphasized by circles, are markers for the spinon configurations (right), where they are reproduced as small circles. Each square on the right represents a spinon. The set of squares is complementary to that of circles with the same range. The number $m_i = 1, 2, \dots, 5$ inside each square marks the spinon orbital. The energy of each S_T multiplet is stated on the far right.

It is useful to introduce spinon orbitals associated with distinct spinon momentum quantum numbers m_i . The wave number of any XXX multiplet can be expressed in terms of the spinon orbital momenta as follows:

$$k = \left(\frac{\pi}{N} \sum_{j=1}^{N_s} m_j - \frac{N\pi}{2} \right) \text{mod}(2\pi). \quad (39)$$

The range of m_i depends on both N and N_s :

$$m_i = \frac{N_s}{2}, \frac{N_s}{2} + 2, \dots, N - \frac{N_s}{2}. \quad (40)$$

The number of available orbits to N_s spinons, $N_{\text{orb}} = (N - N_s)/2 + 1$, thus decreases by one for every two spinons added, $\Delta N_{\text{orb}} = -\Delta N_s/2$, which is one way of recognizing the semionic nature of spinon particles. The exact exclusion statistics of spinons is encoded in the number of ways N_+ spin-up spinons and N_- spin-down spinons can be distributed among N_{orb} accessible orbitals. The spinon multiplicity expression [18],

$$W(N_+, N_-) = \prod_{\sigma=\pm} \binom{d_\sigma + N_\sigma - 1}{N_\sigma}, \quad d_\sigma = A_\sigma - \sum_{\sigma'=\pm} g_{\sigma\sigma'}(N_{\sigma'} - \delta_{\sigma\sigma'}), \quad (41)$$

$$A_\sigma = \frac{1}{2}(N+1), \quad g_{\sigma\sigma'} = \frac{1}{2}, \quad (42)$$

is cast in the same general form as its string counterpart (35). Summation of $W(N_+, N_-)$ over all allowed values of N_\pm accounts for all 2^N states.

The complementary relationship between the string and spinon particles is reflected in their motifs. In Fig. 4 we show the string motif and spinon motif of all 20 S_T -multiplets for $N = 6$ side by side. The number of spinons contained in each eigenstate of a given S_T -multiplet is equal to the number of vacancies left by the 1-string BQN, I_α^1 , across the range (28). In Fig. 4 (right) we have marked the positions of the I_α^1 by circles and the vacancies by squares. The number inside each square denotes the orbital m_i to which every spinon belongs. The available orbitals depend on N_s via (40).

The rules for assigning spinons of particular momentum quantum numbers to orbitals must ensure (i) that the m_i reproduce, via (39), the wave number k already known via (27) and (ii) that the permissible spin orientations are consistent with the quantum number S_T . The allowed combinations of spinon orbitals are encoded in those S_T -multiplets that do not contain any strings with $m > 1$. Here the positions of the 1-strings, i.e. the circles in the spinon motifs, play the role of delimiters between successive spinon orbitals.

A spinon orbital with l_i spinons has an orbital spin $S_i^{\text{orb}} = l_i/2$, $i = 1, \dots, N_{\text{orb}}$. If all N_s spinons are in the same orbital such as in the first two motifs (numbered from top to bottom) this spinon configuration represents a multiplet with $S_T = S_i^{\text{orb}} = N_s/2$. Any distribution of spinons into multiple orbitals represents more than one S_T -multiplet. The multiplets represented are determined via the decomposition of tensor products of orbital spins.

For example, if we have one spinon with $m_i = 2$ and three spinons with $m_i = 4$, that decomposition reads $\frac{1}{2} \otimes \frac{3}{2} = 2 \oplus 1$. The associated multiplets with $S_T = 2$ and $S_T = 1$ are found in motifs three and thirteen, respectively. The configuration with two spinons in each of the same two orbital represents three S_T -multiplets according to $1 \otimes 1 = 2 \oplus 1 \oplus 0$. They are found in motifs four, fourteen, and twenty, respectively. The systematic application of these rules assigns a unique spinon momentum and spin content to every S_T -multiplet.

The energetic split of different S_T -multiplets associated with the same spinon momenta is caused by a coupling between orbital spins. In the Haldane-Shastry model, which has higher symmetry, that coupling is absent and these particular S_T -multiplets remain degenerate [27, 28]. In the XX model, which has lower symmetry, even the S_T -multiplets split up energetically as will be discussed in Sec. 3.3 [14].

The translation and reflection symmetries of \mathcal{H}_{XXZ} dictate that every state with wave number k can be transformed into a state with wave number $2\pi - k$ and the same energy, implying that any state with $k = 0, \pi$ is its own image. These transformation properties are reflected in the string motif ($I_\alpha^m \rightarrow -I_\alpha^m$) and in the spinon motif ($m_i \rightarrow N - m_i$) as is evident in Fig. 4.

3.2. Ising limit: stretched strings, domains, and solitons

In the following we describe three ways of generating the spectrum of the Ising chain, each producing a distinct set of quasiparticles with different exclusion statistics. We begin with the analysis of the string solutions of the BAE from Sec. 2.1. To arrive at a non-divergent spectrum in the Ising limit of \mathcal{H}_{XXZ} we rescale the exchange coupling as follows:

$$\mathcal{H}_I \doteq \lim_{\Delta \rightarrow \infty} \Delta^{-1} \mathcal{H}_{XXZ} = J \sum_{l=1}^N S_l^z S_{l+1}^z. \quad (43)$$

The rescaled energy expression (5) of the Bethe ansatz in raw form thus becomes

$$\frac{E - E_F}{J} = -r + \lim_{\Delta \rightarrow \infty} \sum_{i=1}^r \frac{\cos k_i}{\Delta}. \quad (44)$$

Evidently, real magnon momenta contribute only summarily to the energy, namely via the first term in (44). Non-vanishing terms $\cos k_i/\Delta$ can only come from complex k_i with infinite imaginary parts.

We first track the highest-weight states of the S_T -multiplets from the XXX limit to the Ising limit. For these states, all solutions that are real at $\Delta = 1$ stay real and all solutions that are complex at $\Delta = 1$ have imaginary parts that diverge as $\Delta \rightarrow \infty$. The non-highest-weight states evolve far less uniformly. The additional rapidities, which are all equal to $\pm\infty$ at $\Delta = 1$, become, in general, finite and thus contribute to the energetic split of the S_T -multiplets. In some states, the extra z_i stay real, in other states they combine to form complex pairs. It appears that this transformation from real to complex rapidities takes place throughout the axial regime. Here we focus on the end product at $\Delta = \infty$, where the ferromagnetic domains in Ising product eigenstates become the natural quasiparticles.

Expanding the trigonometric BAE (22) of the axial regime about the Ising limit produces, in leading order, a set of linear BAE for the real parts of the rapidities,

$$\left(N - \sum_{m' \in \mathcal{C}} t_{mm'} n_{m'}\right) z_\alpha^m = 2\pi J_\alpha^m - \sum_{m' \in \mathcal{C}} t_{mm'} \sum_{\alpha'=1}^{n_{m'}} z_{\alpha'}^{m'}, \quad (45)$$

where the new set $\{J_\alpha^m\}$ of BQN, related to the original set $\{I_\alpha^m\}$ by a shift that depends on N and n_m , has the same range (28)

$$|J_\alpha^m| \leq \frac{1}{2} \left(N - 1 - \sum_{m' \in \mathcal{C}} t_{mm'} n_{m'}\right), \quad t_{mm'} \doteq 2\min(m, m') - \delta_{mm'}, \quad (46)$$

which guarantees the correct number of states from the highest-weight type. As the first step in the solution of the linear BAE (45) for these states we introduce the quantities

$$\zeta_m \doteq N - \sum_{m' \in \mathcal{C}} n_{m'} t_{mm'}, \quad J_m \doteq \sum_{\alpha=1}^{n_m} J_\alpha^m, \quad Z_m \doteq \sum_{\alpha=1}^{n_m} z_\alpha^m. \quad (47)$$

Equations (45) summed over α can thus be brought into the form

$$Z_m = 2\pi \frac{J_m}{\zeta_m} - \sum_{m' \in \mathcal{C}} \frac{n_{m'}}{\zeta_m} t_{mm'} Z_{m'} \quad (48)$$

with ζ_m guaranteed to be positive. Equation (48) is solved by matrix inversion. Substitution of the solution Z_m into (45) yields the rapidities

$$z_\alpha^m = 2\pi \frac{J_\alpha^m}{\zeta_m} - \sum_{m' \in \mathcal{C}} \frac{t_{mm'}}{\zeta_m} Z_{m'}. \quad (49)$$

More explicit solutions in compact form for the situations where only 1-strings or only 2-strings are present read

$$z_\alpha^1 = \frac{2\pi}{N-r} J_\alpha^1 - \frac{2\pi}{N(N-r)} J_1, \quad \alpha = 1, \dots, r, \quad (50)$$

$$z_\alpha^2 = \frac{2\pi}{N-3r/2} J_\alpha^2 - \frac{6\pi}{N(N-3r/2)} J_2, \quad \alpha = 1, \dots, r/2. \quad (51)$$

If a single m -string with $1 \leq m \leq N/2$ is present we have $z_1^m = (2\pi/N) J_1^m$ with $|J_1^m| \leq (N-2m)/2$.

In Fig. 5 we have reproduced the BQN of all 20 highest-weight states for $N = 6$ at $\Delta = 1$ from Fig. 4 and have added the BQN for all 22 non-highest-weight states with $M_z \geq 0$. The additional I_α^1 of non-highest-weight states, obtained for $\Delta = 1$ as described at the end of Sec. 2.2, are located beyond the range of the I_α^1 for the highest-weight states (vertical lines).

The choice of the extra I_α^1 and the associated shift of the I_α^m already present is not unique in most cases. Our choice was guided by the aim to avoid multiple I_α^1 of the same value and to restore

			I_α^m							
M_z	S_T	\bar{k}	-3	-2	-1	0	1	2	3	
3	3	0	°	°	°	°	°	°	°	$ 0\rangle$
2	2	5	1	°	°	°	°	°	°	$ 1\rangle$
2	2	4	°	1	°	°	°	°	°	$ 1\rangle$
2	2	3	°	°	1	°	°	°	°	$ 1\rangle$
2	2	2	°	°	°	1	°	°	°	$ 1\rangle$
2	2	1	°	°	°	°	1	°	°	$ 1\rangle$
2	3	0	°	°	°	°	°	°	1	$ 1\rangle$
1	1	2	1	1	°	°	°	°	°	$ 11\rangle$
1	1	1	1	°	1	°	°	°	°	$ 11\rangle$
1	1	0	1	°	°	1	°	°	°	$ 11\rangle$
1	1	0	°	1	1	°	°	°	°	$ 11\rangle$
1	1	5	°	1	°	1	°	°	°	$ 11\rangle$
1	1	4	°	°	1	1	°	°	°	$ 11\rangle$
1	2	5	1	°	°	°	°	1	°	$ 2\rangle$
1	2	4	°	1	°	°	°	1	°	$ 11\rangle$
1	2	3	°	°	1	°	°	1	°	$ 11\rangle$
1	2	2	°	°	°	1	°	1	°	$ 11\rangle$
1	2	1	1	°	°	°	1	°	°	$ 2\rangle$
1	3	0	1	°	°	°	°	°	1	$ 2\rangle$
1	1	4	°	2	°	°	°	°	°	$ 2\rangle$
1	1	3	°	°	2	°	°	°	°	$ 2\rangle$
1	1	2	°	°	°	2	°	°	°	$ 2\rangle$

			I_α^m							
M_z	S_T	\bar{k}	-3	-2	-1	0	1	2	3	
0	0	3	1	1	1	°	°	°	°	$ 111\rangle$
0	1	2	1	1	°	°	1	°	°	$ 12\rangle$
0	1	1	1	°	1	°	1	°	°	$ 12\rangle$
0	1	0	1	°	1	°	°	1	°	$ 12\rangle$
0	1	0	°	1	1	°	1	°	°	$ 111\rangle$
0	1	5	1	°	°	1	°	°	°	$ 12\rangle$
0	1	4	1	°	1	1	°	°	°	$ 12\rangle$
0	2	5	1	°	°	°	1	1	°	$ 3\rangle$
0	2	4	°	1	°	°	1	1	°	$ 12\rangle$
0	2	3	°	°	1	°	1	1	°	$ 12\rangle$
0	2	2	1	°	°	1	°	1	°	$ 12\rangle$
0	2	1	1	°	°	1	°	°	1	$ 3\rangle$
0	3	0	1	°	°	°	°	1	1	$ 3\rangle$
0	0	1	1	2	°	°	°	°	°	$ 12\rangle$
0	0	0	°	12	°	°	°	°	°	$ 12\rangle$
0	0	5	°	2	1	°	°	°	°	$ 12\rangle$
0	1	4	°	2	°	°	1	°	°	$ 3\rangle$
0	1	3	°	°	2	°	1	°	°	$ 12\rangle$
0	1	2	1	°	2	°	°	°	°	$ 3\rangle$
0	0	3	°	°	°	3	°	°	°	$ 3\rangle$

Figure 5. Specification of all XXX eigenstates with $M_z \geq 0$ for $N = 6$ in the string representation (two columns). The quantum numbers M_z , S_T and $\bar{k} \doteq Nk/2\pi$ of each state are stated on the left. The vertical lines indicate the range (28) of the I_α^1 . The positions of the numbers $m = 1, 2, 3$ between the vertical lines represent the values of the I_α^m for the highest-weight states (with $M_z = S_T$). The additional BQN of the non-highest-weight states (with $0 \leq M_z < S_T$) are all located on the outside. In the Ising limit each state evolves into a translationally invariant linear combination of Ising product states with domains of lengths as indicated on the far right in each column.

the symmetry relations described at the end of Sec. 3.1. For states with $k = 0, \pi$, which are their own images under the symmetry transformation, neither goal was fully achievable for $N = 6$. The I_α^1 configurations are asymmetric in several instances and two identical I_α^1 are unavoidable in one instance. These aesthetic flaws pose no problem for what follows.

To the right of each string motif in Fig. 5 we have added another motif in the shape of a ket. It identifies each string solution as tracked from $\Delta = 1$ to $\Delta = \infty$ with an Ising eigenstate as composed of linear combinations of ferromagnetic domains. We have already introduced these domains in the context of Fig. 2. Here we use a notation conducive to linking Ising product eigenstates with obvious domain composition to Bethe eigenstates with specific string structure in the limit $\Delta = \infty$.

Let the set of λ product vectors with $r = N/2 - M_z$ flipped spins that are generated from one such state, $|\sigma_1 \cdots \sigma_N\rangle$, via translations be represented by $\{|\sigma_1 \cdots \sigma_N\rangle\}_\lambda$. Let

$$\left\{ \underbrace{1 \cdots 1}_{\nu_1} \underbrace{2 \cdots 2}_{\nu_2} \underbrace{3 \cdots 3}_{\nu_3} \cdots \right\}_\Lambda \quad (52)$$

represent the set of Λ translationally invariant linear combinations of all product states that contain ν_n domains of length n subject to the constraint $\nu_1 + 2\nu_2 + 3\nu_3 + \cdots = r$. Any set of the latter kind is constructed from one or several sets of the former kind with matching domain content. For $N = 6$

there are seven sets of translationally invariant Ising eigenstates at $M_z \geq 0$ thus constructed:

$$\{|0\rangle\}_1 \xleftarrow{l.c.} \{|\uparrow\uparrow\uparrow\uparrow\uparrow\rangle\}_1; \quad \{|1\rangle\}_6 \xleftarrow{l.c.} \{|\uparrow\uparrow\uparrow\uparrow\downarrow\rangle\}_6; \quad \{|2\rangle\}_6 \xleftarrow{l.c.} \{|\uparrow\uparrow\uparrow\downarrow\downarrow\rangle\}_6; \quad (53a)$$

$$\{|11\rangle\}_9 \xleftarrow{l.c.} \{|\uparrow\uparrow\uparrow\downarrow\downarrow\rangle\}_6, \{|\uparrow\uparrow\downarrow\uparrow\downarrow\rangle\}_3; \quad \{|3\rangle\}_6 \xleftarrow{l.c.} \{|\uparrow\uparrow\downarrow\downarrow\downarrow\rangle\}_6; \quad (53b)$$

$$\{|12\rangle\}_{12} \xleftarrow{l.c.} \{|\uparrow\uparrow\downarrow\downarrow\uparrow\downarrow\rangle\}_6, \{|\uparrow\uparrow\downarrow\uparrow\downarrow\rangle\}_6; \quad \{|111\rangle\}_2 \xleftarrow{l.c.} \{|\uparrow\downarrow\uparrow\downarrow\uparrow\downarrow\rangle\}_2. \quad (53c)$$

In Fig. 5 we have identified each of these 42 states with a particular BAE solution in the limit $\Delta \rightarrow \infty$. The identification is straightforward for the highest-weight states. Each BQN I_α^m represents exactly one domain of size $\mu = m$. However, the evolution of the non-highest-weight states between $\Delta = 1$ and $\Delta \rightarrow \infty$ is far less predictable. The extra BQN are all of the type I_α^1 at $\Delta = 1$ and the associated rapidities are real and infinite. In some cases all extra rapidities stay real. The domain structure of these states is determined by the I_α^m just as in highest-weight states.

However, for the majority of non-highest-weight states some of the rapidities that start out real at $\Delta = 1$ turn into complex-conjugate pairs at $\Delta > 1$ with imaginary parts that diverge as $\Delta \rightarrow \infty$. This metamorphosis necessitates a reconfiguration of the associated BQN (not shown in Fig. 5). Of the 22 non-highest-weight states for $N = 6$ only six do not acquire additional complex rapidities between $\Delta = 1$ and $\Delta \rightarrow \infty$, namely those states for which the string content encoded in the I_α^m matches the domain content encoded in the ket.

The identification of the BAE solutions in the limit $\Delta \rightarrow \infty$ with Ising eigenstates of specific domain content may be less certain in longer chains where states with different $\{\nu_\mu\}$ but equal M_z are degenerate. That is the case for the two sets of states $\{|13\rangle\}_{24}$ and $\{|22\rangle\}_{12}$ in a chain with $N = 8$ sites, for example. However, it seems reasonable to assume that this degeneracy is absent at $\Delta < \infty$ in most if not all cases and thus guarantees that the BAE solutions have, in general, a unique domain content in the limit $\Delta \rightarrow \infty$. Even though the systematics of the transformation of some BAE solutions between $\Delta = 1$ and $\Delta \rightarrow \infty$ appears elusive at present, the systematics of the endproduct, namely the domain structure of the Ising spectrum for arbitrary N , is well known.

An Ising chain of length N can accommodate domains with $\mu = 1, \dots, N-1$ consecutive flipped spins. Domains of size μ are treated as distinct species of independent particles. The capacity for domains is restricted by the relation

$$\sum_{\mu=1}^{N-1} (\mu+1)\nu_\mu \leq N. \quad (54)$$

The total number of Ising eigenstates with domain content $\{\nu_1, \nu_2, \dots\}$ is governed by a multiplicity expression somewhat similar to (35) yet different [26]:

$$W(\{\nu_\mu\}) = \frac{N}{N-r} \prod_{\mu=1}^{N-1} \binom{d_\mu + \nu_\mu - 1}{\nu_\mu}, \quad d_\mu = A_\mu - \sum_{\mu'=1}^{N-1} g_{\mu\mu'}(\nu_{\mu'} - \delta_{\mu\mu'}), \quad (55)$$

$$A_\mu = N - \mu, \quad g_{\mu\mu'} = \begin{cases} \mu', & \mu < \mu', \\ \mu' + 1, & \mu \geq \mu' \end{cases}, \quad r = \sum_{\mu=1}^{N-1} \mu\nu_\mu. \quad (56)$$

The capacity of the system for domains is controlled by A_μ and the statistical interaction between domains by $g_{\mu\mu'}$. All domains have the same energy, J . The statistical mechanics of domains for the Ising chain has been carried out exactly [26], reproducing familiar results.

In the context of Fig. 2 we have already qualitatively described the antiferromagnetic domain walls (solitons) that are complementary to the ferromagnetic domains. Among the four distinct bonds in the general product state $|\sigma_1\sigma_2\cdots\sigma_N\rangle$, the bonds $\uparrow\uparrow, \downarrow\downarrow$ represent solitons with spin $+1/2, -1/2$, respectively, and $\uparrow\downarrow, \downarrow\uparrow$ are vacuum bonds. Close-packed solitons with like spin orientation reside on successive bonds (e.g. $\uparrow\uparrow\uparrow$), whereas close-packed solitons with opposite spin orientation are separated by one vacuum bond (e.g. $\uparrow\uparrow\downarrow\downarrow$). Each of the seven sets of Ising eigenstates (53) contains a specific number of spin-up and spin-down solitons, $(N_+, N_-) =$

$(6, 0), (4, 0), (3, 1), (2, 0), (2, 2), (1, 1), (0, 0)$. All solitons have the same energy, $J/2$. The multiplicity expression for solitons [26],

$$W(N_+, N_-) = \frac{2N}{N - N_a} \prod_{\sigma=\pm} \binom{d_\sigma + N_\sigma - 1}{N_\sigma}, \quad d_\sigma = A_\sigma - \sum_{\sigma'=\pm} g_{\sigma\sigma'}(N_{\sigma'} - \delta_{\sigma\sigma'}), \quad (57)$$

$$A_\sigma = \frac{1}{2}(N - 1), \quad g_{\sigma\sigma'} = \frac{1}{2}, \quad N_a = N_+ + N_-, \quad (58)$$

is similar to expression (41) for spinons. Solitons and spinons are both semions but have different pseudovacua. Whereas the spinon vacuum was found to be unique, the soliton vacuum is twofold, consisting of the two product Néel states, $|\uparrow\downarrow\uparrow\cdots\downarrow\rangle$ and $|\downarrow\uparrow\downarrow\cdots\uparrow\rangle$ or linear combinations thereof. The soliton vacuum, like the spinon vacuum, is realized only in chains with even N .

3.3. XX limit: broken strings, fermions, and spinons

Here we investigate what happens to the highest-weight and non-highest-weight states of the S_T -multiplets in the presence of planar exchange anisotropy, particularly in the limit $\Delta = 0$. We have seen that in the axial regime there exists a tendency for real BAE solutions to become complex. As $\Delta \rightarrow \infty$ all imaginary parts diverge, binding the magnons tightly into domains. In the planar regime, there exists a trend in the opposite direction. At $\Delta = 0$ all BAE solutions can be regularized as stated in Sec. 2.3, making all magnon momenta real. All strings with $m > 1$ break up into 1-strings. The configurations allowed by the set (34) of BQN, which describe regularized solutions, produce the complete spectrum for arbitrary N .

In Fig. 6 we show the configurations of I_α^1 of all 42 eigenstates with $M_z \geq 0$ at $\Delta = 0$ for $N = 6$ in the same sequence as the corresponding S_T -multiplet states at $\Delta = 1$ have been listed in Fig. 5. All multiplet states at $\Delta = 1$ that contain only 1-strings keep the same configuration at $\Delta = 0$. In the other states, all I_α^1 stay in the same position except the pair of I_α^1 that have identical values in Fig. 5. They are replaced in Fig. 6 by a pair of distinct I_α^1 . Furthermore, each I_α^2 in Fig. 5 is replaced by two I_α^1 in Fig. 6 and the one occurrence of a I_α^3 is replaced by three I_α^1 . Whereas the general rules for these substitutions still elude us, the constraints imposed by symmetry and conservation laws eliminate any ambiguity for the case $N = 6$ shown here. The resulting configuration of I_α^1 produces, via (33), the exact configurations of Jordan-Wigner fermion momenta in a periodic chain [19, 21]. The statistical mechanics of the regularized 1-strings is that of a system of free Jordan-Wigner fermions [20].

Each XX eigenstate thus identified by its composition of 1-strings has a unique composition of spinons. The rules for inferring the spinon motif from the string motif are consistent with the rules described in Sec. 2.2 for the case $\Delta = 1$ but there are some noteworthy differences. The lower rotational symmetry at $\Delta = 0$, which splits up the S_T -multiplet degeneracy, makes it possible to assign to each XX state not only a spinon configuration with unique momentum quantum numbers but to the spinons in each orbital also a unique spin orientation.

The spinon motif is encoded in the string motif of each state shown in Fig. 6 as described in the following. (i) Consider the vertical lines dividing the space of the I_α^1 into two domains the inside and the outside, the latter wrapping around at $\pm N/2$. (ii) Every I_α^1 -vacancy (small circle) inside represents a spin-up spinon (marked by a square) and every I_α^1 ('1') outside represents a spin-down spinon (marked by a diamond). (iii) Any number of adjacent spinons in the motif are in the same orbital, i.e. have the same momentum quantum number m_i from the set (40). Two squares or diamonds that are separated by ℓ consecutive '1's have spinon quantum numbers separated by 2ℓ . (iv) The spinon momentum quantum numbers are sorted in increasing order from the line on the left toward the right through the inside domain (m_i^+) and toward the left with wrap-around through the outside domain (m_i^-).

The spinon motif of Fig. 6 establishes the much needed link between spinon motif of the fermion representation at $\Delta = 0$ introduced in Refs. [13, 14] and the spinon motif of the string representation at $\Delta = 1$ introduced in Fig. 5. Unlike the solitons at $\Delta \rightarrow \infty$, the spinons at $\Delta = 0$ are not free. Nevertheless, an exact statistical mechanical analysis of spinons at $\Delta = 0$ is possible

		I_α^m												I_α^m									
M_z	S_T	\bar{k}	-3	-2	-1	0	1	2	3		M_z	S_T	\bar{k}	-3	-2	-1	0	1	2	3			
3	3	0	◻	◻	◻	◻	◻	◻	◻	3+,3+,3+,3+,3+,3+	0	0	3	◻	◻	◻	◻	◻	◻	◻			
2	2	5	1	◻	◻	◻	◻	◻	◻	4+,4+,4+,4+	0	1	2	◻	1	1	◻	◻	◻	5+,5-			
2	2	4	◻	1	◻	◻	◻	◻	◻	2+,4+,4+,4+	0	1	1	◻	1	◻	1	◻	◻	3+,5-			
2	2	3	◻	◻	1	◻	◻	◻	◻	2+,2+,4+,4+	0	1	0	◻	1	◻	1	◻	◻	3+,3-			
2	2	2	◻	◻	◻	1	◻	◻	◻	2+,2+,2+,4+	0	1	0	◻	1	1	◻	◻	◻	1+,5-			
2	2	1	◻	◻	◻	◻	1	◻	◻	2+,2+,2+,2+	0	1	5	◻	1	◻	1	◻	◻	1-,3+			
2	3	0	◻	◻	◻	◻	◻	◻	◻	3+,3+,3+,3+,3+,3-	0	1	4	◻	◻	1	1	◻	◻	1-,1+			
1	1	2	◻	1	1	◻	◻	◻	◻	5+,5+	0	2	5	◻	1	◻	◻	◻	◻	4+,4+,4-,4-			
1	1	1	◻	1	◻	1	◻	◻	◻	3+,5+	0	2	4	◻	◻	1	◻	◻	◻	2+,4+,4-,4-			
1	1	0	◻	1	◻	◻	1	◻	◻	3+,3+	0	2	3	◻	◻	◻	1	◻	◻	2+,2+,4-,4-			
1	1	0	◻	◻	1	1	◻	◻	◻	1+,5+	0	2	2	◻	1	◻	◻	1	◻	2-,2+,2+,4-			
1	1	5	◻	◻	1	◻	1	◻	◻	1+,3+	0	2	1	◻	1	◻	◻	1	◻	2-,2+,2+,2-			
1	1	4	◻	◻	◻	1	1	◻	◻	1+,1+	0	3	0	◻	1	◻	◻	◻	◻	3-,3+,3+,3+,3-,3-			
1	2	5	◻	1	◻	◻	◻	◻	◻	4+,4+,4+,4-	0	0	1	◻	1	1	◻	◻	◻	5+,3-			
1	2	4	◻	◻	1	◻	◻	◻	◻	2+,4+,4+,4-	0	0	0	◻	1	1	◻	◻	◻	1-,5+			
1	2	3	◻	◻	◻	1	◻	◻	◻	2+,2+,4+,4-	0	0	5	◻	◻	1	1	◻	◻	1+,3-			
1	2	2	◻	◻	◻	◻	1	◻	◻	2+,2+,2+,4-	0	1	4	◻	1	◻	◻	◻	◻	2-,4+,4+,4-			
1	2	1	◻	◻	◻	◻	◻	1	◻	2-,2+,2+,2+	0	1	3	◻	◻	1	◻	◻	◻	2-,2+,4+,4-			
1	3	0	◻	◻	◻	◻	◻	◻	◻	3-,3+,3+,3+,3+,3-	0	1	2	◻	◻	1	◻	◻	◻	2-,2+,4+,2-			
1	1	4	◻	1	◻	◻	◻	◻	◻	2-,4+,4+,4+	0	0	3	◻	1	◻	◻	◻	◻	2-,4+,4+,2-			
1	1	3	◻	◻	1	◻	◻	◻	◻	2-,2+,4+,4+													
1	1	2	◻	◻	◻	1	◻	◻	◻	2-,2+,2+,4+													

Figure 6. Specification of all XX eigenstates with $M_z \geq 0$ for $N = 6$ in the string representation (two columns). The quantum numbers M_z , and $\bar{k} \doteq Nk/2\pi$ of each state are stated on the left. Also shown on the left is the quantum number S_T of the multiplet at $\Delta = 1$ from which the state evolved. The states are listed in the same sequence as those in Fig. 5. The positions of the '1' represent the values of the I_α^1 from (34) and constitute the motifs of the (broken) string configuration of the XX eigenstates. The motif of the complementary spinon configuration is marked by the squares (spin-up spinons) and diamonds (spin-down spinons) as explained in the text. The momentum quantum number m_i and the spin orientation σ_i of each spinon present in that state are given to the right of the dual string/spinon motif.

[14]. Away from the Ising limit, the solitons become interacting particles as well. They can be tracked all the way from $\Delta \rightarrow \infty$ to $\Delta = 0$. A comparison between the spinon composition and soliton composition of the XX eigenstates can be found in Ref. [26].

4. Conclusion

The long-established integrability of \mathcal{H}_{XXZ} imposes stringent constraints on the nature of the interaction between quasiparticles of any kind, reducing it, effectively, to two-body scattering events. As a consequence, these quasiparticles have infinite lifetimes and can thus be regarded as structural elements of the XXZ eigenstates. This makes it possible to systematically generate the complete spectrum from the pseudovacuum of one or the other set of quasiparticles.

In this work we have discussed two complementary sets of quasiparticles, one set being the basic elements of string solutions of the coordinate Bethe ansatz and the other the semionic spinons or solitons. Our focus has been on developing interlocking motifs for each set of quasiparticles for the purpose of tracking them across the axial and planar regimes of \mathcal{H}_{XXZ} . Starting from the symmetry point $\Delta = 1$ in parameter space we have identified opposite trends, in the two regimes, in the evolution of string particles, which can be thought of as bound clusters of magnons. In the axial regime, the strings show a tendency of increasing tightness in the binding within each cluster (rapidities with growing imaginary parts) and a tendency of merging clusters (real rapidities

becoming complex). The endproduct at $\Delta = \infty$ are ferromagnetic domains of flipped spins. In the planar regime, the strings appear to loosen up and break apart. At $\Delta = 0$ it is possible to transform away all complex rapidities and with them any trace of magnon clustering. The free magnons behave like hard-core bosons or free fermions.

For $J > 0$ the pseudovacuum of string particles is located at the top of the spectrum throughout the axial regime and then migrates down toward the center of the spectrum in the planar regime. The ground state (physical vacuum) of \mathcal{H}_{XXZ} is unique in the planar regime and twofold in the axial regime. It can be identified as the pseudovacuum of spinons or solitons, respectively. We have given detailed descriptions of spinons at $\Delta = 0$ and $\Delta = 1$ and of solitons at $\Delta = \infty$, including their relationship to the string particles. What remains to be investigated is the metamorphosis of the string particles between the special points $\Delta = 0, 1, \infty$ in parameter space. This is work in progress. Of particular interest is an analysis of the transformations for which we have given here only qualitative descriptions and the impact of these transformations on the motifs such as displayed in Figs. 4-6 including the effects on the complementary spinon and soliton particles.

References

1. Steiner M, Villain J and Windsor C G, 1976 *Adv. Phys.* **25** 87
2. Furrer A (Ed.), *Frontiers in neutron scattering* (World Scientific, Singapore, 2000)
3. Bethe H, 1931 *Z. Phys.* **71** 205
4. Batchelor M T, 2007 *Phys. Tod.* **60/1** 36
5. Lieb E and Liniger W, 1963 *Phys. Rev.* **130** 1605
6. Yang C N and Yang C P, 1969 *J. Math. Phys.* **10** 1115
7. Takahashi M, *Thermodynamics of one-dimensional solvable models* (Cambridge University Press, 1999)
8. Lieb E H and Wu F Y, 1968 *Phys. Rev. Lett.* **20** 1445
9. Essler F H L, Frahm H, Göhmann F, Klümper A et al., *The one-dimensional Hubbard model* (Cambridge University Press, 2005)
10. Bergknoff H and Thacker H B, 1979 *Phys. Rev. Lett.* **42** 135
11. Karbach M and Müller G, 1997 *Comp. in Phys.* **11** 36
12. Biegel D, Karbach M, Müller G and Wiele K, (2004) *Phys. Rev. B* **69** 174404
13. Arikawa M, Karbach M, Müller G and Wiele K, 2006 *J. Phys. A: Math. Gen.* **39** 10623
14. Karbach M, Müller G and Wiele K, 2008 *J. Phys. A: Math. Gen.* **41** 205002
15. Deguchi T, Fabricius K and McCoy B M, 2001 *J. Stat. Phys.* **102** 701
16. Fabricius K and McCoy B M, 2001 *J. Stat. Phys.* **103** 647
17. Fabricius K and McCoy B M, 2001 *J. Stat. Phys.* **104** 573
18. Haldane F D M, 1991 *Phys. Rev. Lett.* **67** 937
19. Lieb E, Schulz T and Mattis D, 1961 *Ann. Phys.* **16** 407
20. Katsura S, 1962 *Phys. Rev.* **127** 1508
21. McCoy B M, Barouch E and Abraham D B, 1971 *Phys. Rev. A* **4** 2331
22. Derzhko O, 2002 *Cond. Mat. Phys.* **5** 729
23. des Cloizeaux J and Gaudin M, 1966 *J. Math. Phys.* **7** 1384
24. Wu Y S, 1994 *Phys. Rev. Lett.* **73** 922
25. Frahm H and Stahlsmeier M, 1998 *Phys. Lett. A* **250** 293
26. Lu P, Vanasse J, Piecuch C, Müller G et al., 2008 *J. Phys. A: Math. Gen.* **41** 265003
27. Haldane F D M, 1988 *Phys. Rev. Lett.* **60** 635
28. Shastri B S, 1988 *J. Stat. Phys.* **50** 57